

2010-01-01

Multiple Scattering from Bubble Clouds

Xiaojun Chen

University of Miami, x.chen10@miami.edu

Follow this and additional works at: https://scholarlyrepository.miami.edu/oa_theses

Recommended Citation

Chen, Xiaojun, "Multiple Scattering from Bubble Clouds" (2010). *Open Access Theses*. 36.
https://scholarlyrepository.miami.edu/oa_theses/36

This Open access is brought to you for free and open access by the Electronic Theses and Dissertations at Scholarly Repository. It has been accepted for inclusion in Open Access Theses by an authorized administrator of Scholarly Repository. For more information, please contact repository.library@miami.edu.

UNIVERSITY OF MIAMI

MULTIPLE SCATTERING FROM BUBBLE CLOUDS

By

Xiaojun Chen

A THESIS

Submitted to the Faculty
of the University of Miami
in partial fulfillment of the requirements for
the degree of Master of Science

Coral Gables, Florida

May 2010

©2010
Xiaojun Chen
All Rights Reserved

UNIVERSITY OF MIAMI

A thesis submitted in partial fulfillment of
the requirements for the degree of
Master of Science

MULTIPLE SCATTERING FROM BUBBLE CLOUDS

Xiaojun Chen

Approved:

Thomas Hahn, Ph.D.
Assistant Professor of
Applied Marine Physics

Terri A. Scandura, Ph.D.
Dean of the Graduate School

Michael Brown, Ph.D.
Professor of
Applied Marine Physics

Mohamed Iskandarani, Ph.D.
Associate Professor of
Meteorology and
Physical Oceanography

CHEN, XIAOJUN

Multiple Scattering From Bubble Clouds

(M.S., Applied Marine Physics)

(May 2010)

Abstract of a thesis at the University of Miami.

Thesis supervised by Professor Thomas Hahn.

No. of pages in text. (39)

Multiple scattering effects from bubble clouds are investigated in this study. A high performance, general purpose numerical tool for multiple scattering calculations is developed. This numerical tool is applied in three computational scenarios in this study. The total scattering cross section of a bubble cloud is investigated. Numerical results indicate that the resonant frequency of the bubble cloud is much lower than that of a single bubble. The variation of resonant frequency of multiple scattering is also studied. It is found that the resonant frequency decreases as the number of bubbles increases, or as the void fraction of the bubble cloud decreases. Phase distributions of bubble oscillations in various multiple scattering scenarios are presented. It is found that, at resonance, the bubbles synchronize to the same phase, which is indicative of the lowest mode of collective oscillation. At wave localization, half of the bubbles oscillate at phase 0 while the other half oscillate at phase π . An intuitive interpretation of this behavior is given.

Acknowledgement

This study is carried out under the supervision of Prof. Thomas Hahn. I would like to thank him for his patience, encouragement, and great care in advising my master's study. This work could not have been done without his professional knowledge in the area and his guidance in giving me directions.

Financial support for this work is mainly provided by ONR, under grant number N000140710896.

Deep appreciation is also expressed to my other committee members, Prof. Michael Brown, who has been very supportive throughout my study in University of Miami, and Prof. Mohamed Iskandarani, who has given me great help in developing my code.

Last but not the least, I would like to thank my parents. It's their love, encouragement, and support that make my life more enjoyable.

TABLE OF CONTENTS

	Page
LIST OF FIGURES	v
Chapter	
1 Introduction	1
2 Background	7
3 Methods and Numerical Computation	11
3.1 Linear Bubble Dynamics.....	11
3.2 Scattering Function of the Bubble	13
3.3 Numerical Computation Approach	16
3.4 Optimization of Code	20
3.4.1 LAPACK Subroutine	20
3.4.2 MPI Parallelization	21
4 Computation Scenarios.....	23
4.1 Scattering Cross Section for Large Number of Bubbles.....	23
4.2 Resonant Frequency Shift	26
4.3 Phase Distribution.....	30
5 Summary	36
Bibliography	38

List of Figures

1	Pressure inside and outside the bubble.....	13
2	Geometry of the multiple scattering problem	16
3	Total scattering cross section of an assemblage consisting of 3000 bubbles .	24
4	Directivity of assemblage scattering at 100, 478, 1000, 2000 Hz.....	25
5	Total scattering cross section for an assemblage of 500 bubbles at different void fraction values.....	28
6	Resonant frequency of the assemblage as a function of void fraction	29
7	Total scattering cross section as a function of ka for 3,000 bubbles	31
8	Phase distribution of the 3,000 bubbles at two resonant peaks in Figure 7	32
9	Total field intensity (compensated by distance) as a function of frequency ..	33
10	Phase distribution at frequencies marked in Figure 9.....	34

Chapter 1 Introduction

Due to the great difference in acoustic impedance between air and water, bubbles, as highly effective scatterers, have received a lot of attention in the study of underwater acoustics, ultrasound imaging, etc.

The behavior of a single bubble in the sound field is well understood. As early as 1933, Minnaert (Minnaert, 1933) proposed his equation for the bubble's natural frequency:

$$\omega_0 = \frac{1}{a} \sqrt{\frac{3\gamma p_0}{\rho_w}} . \quad (1)$$

Here, a is the radius of the bubble and p_0 is the static pressure at the equilibrium state; ρ_w is the density of water; and γ is the polytropic index of the gas inside the bubble. The derivation of this equation basically treats the bubble in analogy to a spring. Damping effects can also be incorporated to determine the natural frequency (Leighton, 1994). Detailed linear bubble dynamics will be discussed in later chapters. Typically, with $p_0 = 10^5 \text{ Pa}$, $\rho = 10^3 \text{ kg/m}^3$, and $\gamma = 1.4$, bubbles with a radius of 7 mm would resonate at the frequency of 500 Hz; bubbles of 1 mm radius would resonate at 3.3 kHz.

In most scenarios of interest, we are usually dealing with collections of bubbles, i.e. bubble clouds, rather than a single bubble. For example, in ultrasound imaging, contrast agents are used to produce masses of micro bubbles in certain areas (organs), so that more backscattering can be achieved to distinguish them from normal tissues. Also, in

ocean acoustics, the surface layer contains of large amount of bubbles, which might be generated by breaking waves, surface turbulence, and water drop impact (Prosperetti A. , 1988).

In some of the cases mentioned above, there is no need to account for the multiple scattering effects from bubbles. For example, in ultrasound imaging, when the concentration of the micro bubbles is relatively low, the scattered field can simply be computed by adding up all the scattering waves from each bubble. This can be argued to be reasonable when concentration is low and the bubbles are far away from each other; then the interaction between bubbles does not play an important role.

However, as concentrations go up, the distances between bubbles become small, so more interaction can be expected and multiple scattering effects cannot be ignored any more. This view is supported by much research done in the past decades. For example, in a series of experiments conducted by Hughes *et al* (Hughes, Klivanov, Marsh, Miller, & Brandenburger, 2000) to measure the attenuation and phase velocity parameters on Albunex[®] (one of the contrast agents widely used in ultrasound imaging) suspensions , it was found that when the concentration of Albunex[®] exceeds 107 particles/ml, the peak attenuation would shift towards higher frequencies. Also, Zhang *et al* (Zhang, Gong, Liu, Shao, Li, & Zhang, 2000) reported an unusual increase in non-linear parameter as the concentration of contrast agent particles go up, which was ascribed to the multiple scattering effects.

Moreover, it is also well known that bubbles play an important role in oceanic ambient noise (Wenz, 1962). As mentioned earlier, bubbles are abundant on the surface layer of the ocean. They are created in various ways, like by biological activities, by drop impacts such as rain, spays, and most importantly by breaking waves. Different mechanisms contribute to different frequency ranges (Prosperetti A. , 1988). For example, amplification of water turbulence by bubbles is believed to be responsible for the frequency range from a few Hz to 100-200 Hz; individual freely oscillating bubbles, on the other hand, contributes to the range from 1 to 10 kHz. However, it is found that the ambient noise spectra exhibits a broad maximum at frequencies around 500 Hz, which could not be explained by scattering from individual bubbles. The formula we presented earlier demonstrates it very well. In order to produce a natural frequency of 500 Hz, bubbles need to have a radius of 7 mm. It is unlikely that such large bubbles could have been generated in large amounts in the ocean under any conditions.

The frequency range around 500 Hz, on the other hand, can be well predicted by the mechanism of multiple scattering. Prosperetti (Prosperetti A. , 1988) estimated that the collective modes of bubbles can easily go down to several hundred Hz. S. W. Yoon et al (Yoon, Crum, Prosperetti, & Lu, 1991) also experimentally demonstrated the existence of collective modes at a few hundred Hertz.

In summary, multiple scattering effects play an important role in many research areas. Better understanding toward the mechanism of multiple scattering will help us interpret many phenomena that cannot be explained otherwise.

Various theories have been proposed to account for the multiple scattering effects (Foldy, 1945) (Twersky, 1962). Among them, the most widely used is Foldy's effective medium theory. In Foldy's pioneering paper (Foldy, 1945), he proposed that the whole bubble cloud can be treated as a single scattering object, with uniform acoustic properties, i.e., wave number, sound speed, etc. According to Foldy's self-consistent theory, the well-known dispersion relationship is derived:

$$k_e^2 = k^2 + 4\pi n f_s , \quad (2)$$

where k_e is the effective wave number, n is the volume density of the scatterers, and f_s is the scattering amplitude of a single scatterer. Foldy's effective medium theory has been experimentally verified to hold in most cases except at frequencies near the bubble's resonance frequency (Commande & Prosperetti, 1989). Hahn's work (Hahn, 2007), which used the effective medium theory to compute low frequency sound scattering from spherical assemblages of bubbles, also confirmed the validity of Foldy's theory -- analytical results are found to agree very well with that produced from first-principle numerical computations. It should be noted that higher order corrections are also proposed by Ye and Ding (Ye & Ding, 1995), Henyey (Henyey, 1999) to incorporate more complicated scattering processes.

In the framework of Foldy's effective medium theory, many interesting topics have been explored. Hahn (Hahn, 2007) noted that the peak frequency for the cross section of the bubble assemblage would shift to lower frequencies as the assemblage becomes denser. But no further insight is provided regarding the relationship among the peak

frequency, the number of bubbles, and the density of the bubbles. What would the relationship be? Are they strongly related to each other?

Another interesting topic also arises in the work of Ye, Hsu & Hoskinson (Ye, Hsu, & Hoskinson, 2000). In that paper, it is shown by numerical simulation that all scatterers tend to synchronize their phases when an acoustic “localization” phenomenon is observed. The term “localization” is in analogy to the famous “electron localization” effect first found by Anderson in 1958 (Anderson P. W., 1958), since in both cases, the phenomenon that energy is trapped locally by the random scatterers, either impurities or bubbles, is observed. Though the research is done in 2D, it certainly provides us a new perspective to understand the physics involved in multiple scattering processes. What happens in the 3D problem? What about the phases at other special circumstances, like resonance? Why would the phases synchronize? All these questions remain open questions.

While analytical methods are very difficult to apply for the physics of multiple scattering problems, numerical calculation, using effective medium theory, becomes a very powerful tool to predict the scattered field around the assemblage. Hahn employed effective medium theory to numerically calculate the scattering cross section around a spherical assemblage (Hahn, 2007). Hoskinson & Ye also used numerical simulation to investigate phase transitions in a 2D assemblage (Hoskinson & Ye, 1999). However, they were able to handle only small numbers of scatterers, due to the limitations in computational resources and inefficient numerical algorithms.

The objective of my research is to develop a high performance numerical program for multiple scattering problems, which could be used for general purpose calculations, regardless of assemblage shape, number of scatterers, positions of the scatterers being periodic, fixed, or even random, cross section or phase distribution or other quantities to be calculated. The numerical calculation would basically follow Foldy's self-consistent effective medium theory. Moreover, it will follow the very first principles of the multiple scattering process, and thus reveal some of the facts that are hidden in the effective medium theory, like the states of each oscillating bubble inside the assemblage. We would use this model to provide some new insights on topics including: cross section of assemblage with large number of bubbles; resonance frequency shift due to variance in volume fraction and number of bubbles in the cloud; phase state distribution of the bubbles in special circumstances, such as resonance, localization, etc. We are hoping that this numerical model would be of good help in enhancing our understanding of multiple scattering problems.

In the following chapters, we will first cover the background theories of this work in Chapter 2, introducing Foldy's effective medium theory and corrections to it. In chapter 3, we will talk about the methods that have been used, for example, how the numerical calculation method is derived, what is the scattering function of a single bubble, and also the optimizations that are used in the code. Chapter 4 will deal with 3 specific computation scenarios. Computation results are given in plots and interpretation of the results is also provided. Chapter 5 summarizes the work presented and gives conclusions based on the earlier chapters.

Chapter 2 Background

In this chapter, we present the background theories that lay the foundation for the later computations. We will mainly cover Foldy's effective medium theory.

As early as 1945, Foldy proposed a way to treat the multiple scattering problems involving an assemblage of scatterers (Foldy, 1945), the effective medium theory. His pioneering work has been widely used in many areas where multiple scattering process is involved.

Foldy's effective medium theory is basically a statistical treatment of the problem. In Foldy's theory, for a cloud of scatterers randomly distributed in space, one is not interested in the values of physical quantities for a specific configuration, but rather in the average value of these quantities being taken over all possible configurations, i.e. the configurational average:

$$\langle f \rangle = \int \dots \int \int f(r_j, s_j) P(r_j, s_j) ds_1 ds_2 \dots ds_N dr_1 dr_2 \dots dr_N \quad (3)$$

Here f is the physical quantity to be averaged, $P(r_j, s_j)$ is the probability distribution function so that $P(r_j, s_j) ds_1 ds_2 \dots ds_N dr_1 dr_2 \dots dr_N$ represents the probability of finding the scatterer 1 in the space range of dr_1 around the point r_1 and has a scattering parameter lying between s_1 and s_1+ds_1 ; scatterer 2 in the space range of dr_2 around the point r_2 and has a scattering parameter lying between s_2 and s_2+ds_2 , etc.

For a particular configuration of scatterers, the acoustic pressure at position r , denoted as $\psi(r)$ satisfies the wave equation

$$\nabla^2\psi + k^2\psi = 0, \quad (4)$$

where k is the wave number and $k = \omega/c$ (c is the phase velocity and ω is the frequency).

$\psi(r)$ can be treated as a sum of incoming wave field and the scattering field by the assemblage, written as

$$\psi(r) = \psi_0(r) + \sum_j f_j \psi^j(r_j) G(r, r_j), \quad (5)$$

$$\psi^j(r_j) = \psi_0(r_j) + \sum_{i \neq j} f_i \psi^i(r_i) G(r_j, r_i). \quad (6)$$

Here, ψ_0 is the incoming wave function, f_j is the scattering coefficient for the j th scatterer, and $G(r, r_j)$ is the free space Green's function. $\psi^i(r_i)$ is defined as the external field acting on the j th scatterer, which is also decomposed into the incoming wave field at r_j and the scattering field at r_j from all the other scatterers.

Now Let us compute the configurational average of $\psi(r)$. Averaging both sides of equation (5), we have

$$\langle \psi(r) \rangle = \langle \psi_0(r) \rangle + \sum_j \iint f_j \langle \psi^j(r_j) \rangle G(r, r_j) P(r_j, s_j) dr_j s_j. \quad (7)$$

According to the definition, $\langle \psi^j(r_j) \rangle$ represents the external field acting on the j th scatterer. Since the difference between $\langle \psi^j(r_j) \rangle$ and the configurational average of the

actual field at r_j , denoted as $\langle \psi(r_j) \rangle$, is just a term of order $1/N$, when N is large enough, the difference could be omitted and we may replace $\langle \psi^j(r_j) \rangle$ in equation (7) with $\langle \psi(r_j) \rangle$. Also, notice that the configurational average of $\psi_0(r)$ is just $\psi_0(r)$ itself, and the probability distribution function $P(r_j, s_j)$ is defined as

$$P(r_j, s_j) = \frac{n(r_j, s_j)}{N}, \quad (8)$$

where $n(r_j, s_j)$ is defined as the average number of scatterers in the neighborhood of r_j having scattering parameters s_j . So equation (7) can now be rewritten as

$$\begin{aligned} \langle \psi(r) \rangle &= \psi_0(r) + \sum_j \iint f_j \langle \psi^j(r_j) \rangle G(r, r_j) \frac{n(r_j, s_j)}{N} dr_j s_j \\ &= \psi_0(r) + \sum_j \iint f_j \langle \psi(r_j) \rangle G(r, r_j) \frac{n(r_j, s_j)}{N} dr_j s_j \\ &= \psi_0(r) + \int F(r') \langle \psi(r') \rangle G(r, r') dr', \end{aligned} \quad (9)$$

where $F(r)$ is defined as

$$F(r) = \int f_j n(r, s) ds. \quad (10)$$

To derive the wave equation for the configurational averaged quantity of $\langle \psi(r) \rangle$, we now apply the operator $\nabla^2 + k^2$ on both sides of equation (9)

$$\begin{aligned} (\nabla^2 + k^2) \langle \psi(r) \rangle &= (\nabla^2 + k^2) \psi_0(r) \\ &\quad + (\nabla^2 + k^2) \int F(r') \langle \psi(r') \rangle G(r, r') dr' \end{aligned} \quad (11)$$

On the left side, the first term $(\nabla^2 + k^2) \psi_0(r)$ is 0, since the incoming wave $\psi_0(r)$ should satisfy the wave equation. For the second term, according to the definition of free space Green's function,

$$(\nabla^2 + k^2)G(r, r_j) = -4\pi\delta(r, r_j). \quad (12)$$

So now we can write equation (11) as

$$(\nabla^2 + k^2)\langle\psi(r)\rangle = -4\pi F(r)\langle\psi(r)\rangle. \quad (13)$$

We may rewrite equation (13) in wave equation form:

$$(\nabla^2 + k_e^2)\langle\psi(r)\rangle = 0, \quad (14)$$

where

$$k_e^2 = k^2 + 4\pi F(r). \quad (15)$$

If the N isotropic scatterers are randomly distributed, $F(r) = Nf_s$. So the effective wave number k_e could be obtained as

$$k_e^2 = k^2 + 4\pi Nf_s. \quad (16)$$

Here f_s is the scattering amplitude of a single scatterer. Equation (16) is the famous Foldy effective wave number that is widely used in many applications.

Chapter 3 Methods and Numerical Computation

In this chapter, we will present the theoretical basis for the approach used in our numerical algorithm. We start from linear bubble dynamics, and then consider the scattered field of a single bubble. Finally we will discuss our numerical computation approach for multiple scattering problems.

3.1 Linear bubble dynamics

The understanding of bubble dynamics is essential in multiple scattering problems. For simplicity, we are concerned with the linear, rather than nonlinear, bubble dynamics in this research.

The classic approach used in linear bubble dynamics is the mass spring model. Consider the pulsating bubble as a vibrating spring with certain mass and stiffness. Of course, there are different ways to define parameters like mass and stiffness, due to different definitions of driving force and displacement. For example, the driving force could be defined either as acoustic pressure or as the force exerted on the surface; the displacement could also be defined either as the volume contraction/expansion or the radius away from the equilibrium state. In this article, we will consistently define the physical parameters regarding acoustic pressure as driving force and the changing volume as displacement. The equation of motion for a single bubble can be written as:

$$m\ddot{u} + b\dot{u} + \kappa u = p_0 e^{i\omega t}. \quad (17)$$

Here u is the expansion/extraction volume from the equilibrium state; m is the effective mass of the bubble, $m=\rho/4\pi a$; b describes the damping effects of the bubble, which includes radiation damping, thermal damping, and viscous damping; κ is the stiffness factor, $\kappa=3\gamma p_0/4\pi a^3$; p_0 and ω are the amplitude and frequency of the incoming wave pressure.

From equation (17), we can easily derive the Minnaert's resonant frequency:

$$\omega_0 = \sqrt{\frac{\kappa}{m}} = \frac{1}{a} \sqrt{\frac{3\gamma p_0}{\rho_w}}. \quad (18)$$

The solution to that equation is immediately derived:

$$u = \frac{p_0/\omega^2 m}{\left[\frac{\omega_0^2}{\omega^2} - 1\right] + i \frac{b}{m\omega}}. \quad (19)$$

The imaginary part $\frac{b}{m\omega}$ in the denominator is interpreted as the damping factor, and can be attributed to three major damping mechanisms: re-radiation damping, thermal damping, and viscous damping.

$$\begin{aligned} \delta &= \frac{b}{m\omega} = \delta_{rad} + \delta_{visc} + \delta_{th} \\ &= ka + \frac{4\mu}{\rho\omega a^2} + \frac{P_0}{\rho\omega^2 a^2} Im(\phi). \end{aligned} \quad (20)$$

Generally speaking, the re-radiation part is responsible for the energy re-radiated by the bubble as a vibrating source; the viscous damping is responsible for the energy dissipated by viscosity around the bubble; and the thermal damping is responsible for the loss of heat to the medium in the process of expansion and contraction.

3.2 Scattering function of the bubble

Bubbles are very effective scatterers in the ocean due to the high contrast of ρc between air and water ($\rho c_w / \rho c_{air} = 5000$). The scattering function is relatively easy to obtain because of bubble's spherical shape.

The wavelength for a 500 Hz wave in the ocean is about 3 m, while the radius of a bubble is typically 0.01 m. We can safely treat the bubble as a spherically symmetric scatterer in the sound field. As the bubble oscillates, the wave is radiated out like a monopole source. How do we determine the scattering amplitude if we know the incoming wave amplitude, i.e. what is the scattering function of the bubble?

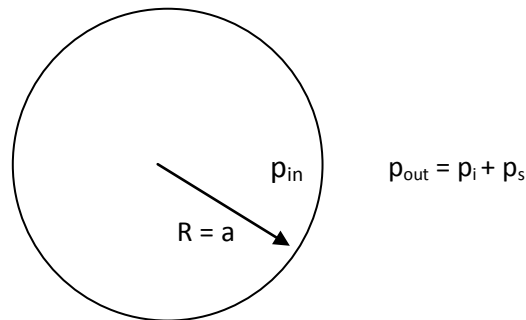


Fig. 1 Pressure in and out of the bubble.

As shown in Fig. 2, the pressure in and out of the bubble should be equal:

$$p_{in} = p_{out} = p_i + p_s \quad (21)$$

Since the scattering wave p_s is originated from the oscillation of the bubble surface, the radial component of the particle speed at the surface can be related to the pressure of the scattering wave p_s :

$$u_{r=a} = -i \frac{P_s}{\rho_w c k a^2} e^{i\omega t}. \quad (22)$$

P_s is the amplitude of the scattering wave p_s .

Also, assuming the gas inside the bubble is ideal and no heat is exchanged, we have

$$PV^\gamma = \text{const}, \quad (23)$$

where P is composed of two parts, the static pressure p_0 and the deviation pressure p_{in} .

Differentiating volume V with respect to time t in equation (23) gives

$$\frac{dV}{dt} = -\frac{i\omega p_{in} V}{\gamma p_0}. \quad (24)$$

Using $dV/dt = 4\pi a^2 u_{r=a}$, we again get another expression of $u_{r=a}$ in terms of p_{in}

$$u_{r=a} = -i \frac{\omega a P_{in}}{3\gamma p_0} e^{i\omega t}. \quad (25)$$

After combining equation (22) and equation (25), and inserting equation (18) for the natural frequency of the bubble, we get the relationship between p_{in} and P_s

$$\frac{P_{in}}{P_s} = \frac{3\gamma P_0}{\rho_w c^2 k^2 a^3} = \frac{1}{a} \left(\frac{\omega_0}{\omega} \right)^2. \quad (26)$$

At the surface, the scattering wave p_s can be expanded using Taylor's expansion

$$p_s = \frac{P_s}{a} e^{ika} e^{i\omega t} = \frac{P_s}{a} (1 - ika) e^{i\omega t}. \quad (27)$$

Later we will see that the $-ika$ term contribute to the damping effect, the so called radiated damping.

Inserting equation (26) and (27) into equation (21) gives

$$P_s = \frac{-a}{\left[\left(\frac{\omega_0}{\omega}\right)^2 - 1\right] + i\delta} P_i. \quad (28)$$

Here δ is the damping term. In our derivation, only radiation term is taken into consideration, $\delta = -ka$. See Clay & Medwin's book (Clay & Medwin, 1977) for a more complete discussion.

The scattering function now can be written as

$$p_s = f_s G(k, r) p_i, \quad (29)$$

where

$$f_s = \frac{-a}{\left[\left(\frac{\omega_0}{\omega}\right)^2 - 1\right] + i\delta}. \quad (30)$$

Note that when we use the free space Green's function, an implicit assumption is the far field approximation. In our computation, we assume that the distance between bubbles are large compared with the radius of the bubble.

According to the above equations, the scattering cross section is

$$\sigma_s = \frac{4\pi a^2}{\left[\left(\frac{\omega_0}{\omega}\right)^2 - 1\right]^2 + \delta^2}. \quad (31)$$

Notice that the cross section that we computed in this research is the total scattering cross section, which incorporates both scattering cross section and extinction cross section. The extinction cross section describes the energy dissipation due to the scattering process.

3.3 Numerical computation approach

In this section, we derive the computational approach that we used to numerically solve the multiple scattering problems. The derivation basically follows Foldy's effective medium theory. Moreover, it follows the first principles of the multiple scattering process, so that we are able to monitor the amplitude and phase of each scatterer as they oscillate.

Let us first define the problem.

As mentioned in the introduction, our numerical program could be applied in various configurations, like periodic units, different shapes of assemblages, also the positions of the scatterers could either be fixed or random. For demonstration purposes, in the following discussion, we will work on a spherical assemblage with N bubbles randomly distributed inside, a configuration shown in Fig. 2.

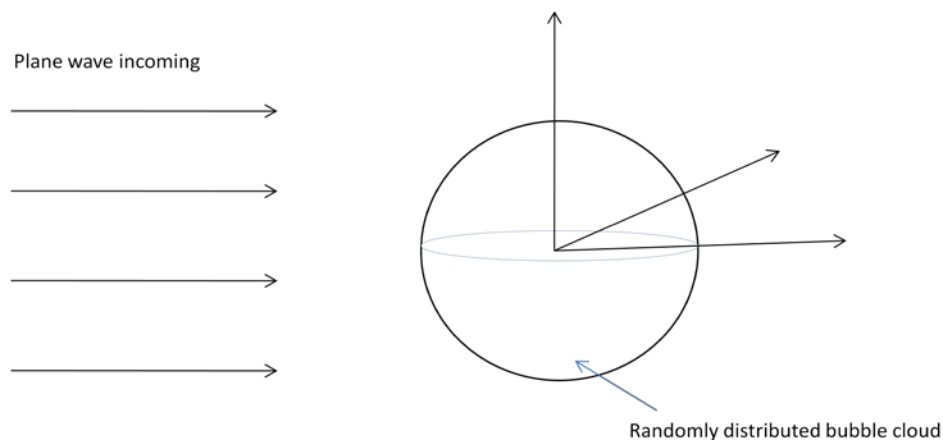


Fig. 2 Geometry of the multiple scattering problem.

For simplicity, all N bubbles are assumed to be the same. The position of the i th bubble is denoted as \mathbf{r}_i , $i=1, 2, \dots, N$. The incident wave is set to be a plane wave,

$$p_{inc}(\mathbf{r}) = p_{i0} e^{i(\omega t - k\mathbf{r})}. \quad (32)$$

The receivers are placed far away, a distance 10 times the assemblage radius, making sure that we are calculating the far field.

The total field at the receiver \mathbf{r} is given by:

$$p(\mathbf{r}) = p_{inc}(\mathbf{r}) + p_s(\mathbf{r}), \quad (33)$$

which is composed of the incoming field $p_i(\mathbf{r})$ and scattering field $p_s(\mathbf{r})$. The scattering field $p_s(\mathbf{r})$ is the main problem to tackle. In calculating $p_s(\mathbf{r})$, rather than treating the assemblage as a uniform effective medium, we instead follow the first principles of the multiple scattering process among bubbles, which is explained below.

Basically, this method deals with the behavior of each of the N bubbles, rather than the endless transmission ray path among bubbles. Just as Foldy derived in his effective medium theory, the scattering field of the whole assemblage is the sum of scattering field from all the bubbles in the assemblage:

$$p_s(\mathbf{r}) = \sum_{i=1}^N p_{si}(\mathbf{r}). \quad (34)$$

$p_{si}(\mathbf{r})$ here denotes the scattering field from the n^{th} bubble at \mathbf{r} . Since we already know the scattering coefficient of a single bubble, it only remains to find the incoming wave on each bubble in order to determine p_{si} .

Assuming that the wave scattered by the j^{th} ($j = 1, 2 \dots N$) bubble would not be scattered back to itself by other bubbles in the future, we can basically divide the incoming wave $p^j(\mathbf{r}_j)$ on the j^{th} bubble into two parts:

$$\begin{aligned}
 p^1(\mathbf{r}_1) &= p_{inc}(\mathbf{r}_1) + \sum_{i=2}^N f_s p^i(\mathbf{r}_i) G(k; \mathbf{r}_1 - \mathbf{r}_i) \\
 p^2(\mathbf{r}_2) &= p_{inc}(\mathbf{r}_2) + \sum_{\substack{i=1 \\ i \neq 2}}^N f_s p^i(\mathbf{r}_i) G(k; \mathbf{r}_2 - \mathbf{r}_i) \\
 &\dots \\
 p^j(\mathbf{r}_j) &= p_{inc}(\mathbf{r}_j) + \sum_{\substack{i=1 \\ i \neq j}}^N f_s p^i(\mathbf{r}_i) G(k; \mathbf{r}_j - \mathbf{r}_i)
 \end{aligned} \tag{35}$$

\mathbf{r}_j denotes the position of the j^{th} bubble. The first part $p_{inc}(\mathbf{r}_j)$ is the direct incoming wave field at position \mathbf{r}_j ; the second part, on the other hand, is the sum of scattering waves from all the other bubbles ($i = 1, 2, \dots N$; $i \neq j$) at position \mathbf{r}_i , denoted as $p^i(\mathbf{r}_i)$.

The second part here is the key point in our computation. Another way to interpret it is to take the j^{th} bubble out of the assemblage, as if it was not there. This way we can deduce the incoming wave on the j^{th} bubble, by summing the direct incoming wave part $p_i(\mathbf{r}_j)$ and all the scattered waves from the rest of the bubbles.

We now have N linear equations and also N unknowns $p^j(\mathbf{r}_j)$, $j = 1, 2 \dots, N$. These equations can be written in matrix form:

$$p^j = p_{inc}(\mathbf{r}_j) + f_s \mathbf{G}^k p^j \tag{36}$$

The matrix $G_{i,j}^k$ is defined as a $N \times N$ matrix:

$$G_{i,j}^k = \begin{cases} G(k; \mathbf{r}_i - \mathbf{r}_j), & i \neq j \\ 0, & i = j \end{cases} . \tag{37}$$

According to the definition, $G_{i,j}^k$ is a complex symmetric matrix, since the source and the receiver \mathbf{r}_j in the free space Green's function can be interchanged, or more generally by reciprocity. Complex symmetry is an important feature of $G_{i,j}^k$, which will simplify the computational task of computing its inverse. Note that when we use the free space Green's function, an implicit assumption is the far field approximation. If \mathbf{r}_i and \mathbf{r}_j are too close to each other, the free space Green's function cannot be applied any more. Here we assume that \mathbf{r}_i and \mathbf{r}_j are far away from each other, compared with the radius of the bubble. In typical computation, the radius of the bubble is 0.01 m, while the average distance between bubbles is 0.15 m.

The matrix form equation can be easily solved with matrix inversion,

$$p^j(\mathbf{r}_j) = (\mathbf{I} - f_s \mathbf{G}^k)^{-1} p_{inc}(\mathbf{r}_j). \quad (38)$$

The total scattering field $p_s(\mathbf{r})$ is given by

$$p_s(\mathbf{r}) = \sum_{i=1}^N f_s p^i(\mathbf{r}_i) G(k; \mathbf{r} - \mathbf{r}_i) \quad (39)$$

Insert equation (34) into equation (35) and (38), and change the summation operation into matrix multiplication. Now we have the solution to the coupled scattering field problem:

$$\begin{aligned} p(\mathbf{r}) &= p_{inc}(\mathbf{r}) + p_s(\mathbf{r}) \\ &= p_{inc}(\mathbf{r}) + f_s [(\mathbf{I} - f_s \mathbf{G}^k)^{-1} p_i(\mathbf{r})]^T \cdot \mathbf{G}^k(\mathbf{r}). \end{aligned} \quad (40)$$

The vector $\mathbf{G}^k(\mathbf{r})$ is defined as

$$\mathbf{G}^k(\mathbf{r}_i) = G(k; \mathbf{r} - \mathbf{r}_i). \quad (41)$$

Now with the help of equation (40), we can numerically calculate many quantities of interest.

3.4 Optimization of code

In order to calculate as many scatterers as possible, we have used an LAPACK subroutine to solve the matrix equation; we have also written a parallel version of our code so that it could be run on multiple processors at the same time.

3.4.1 LAPACK Subroutine

The most time consuming part of the simulation is the matrix inverse operation in equation (38).

Initially, we tried the standard Gaussian elimination solver, provided in Numerical Recipes in C (Press, Teukolsky, Vetterling, & Flannery, 1992). It does the job, but not fast enough. For example, for a cloud of 1000 bubbles, it takes 97 hours to finish 300 configurations on a single processor from Kronos cluster.

Since the matrix to be inverted, $\mathbf{I} - f_s \mathbf{G}_{i,j}^k$, is complex and symmetric, we decided to switch to another matrix solver `zsysv`, which is included in the LAPACK.

LAPACK is the Linear Algebra PACKage that “provides routines for solving systems of simultaneous linear equations, least-squares solutions of linear systems of equations, eigenvalue problems, and singular value problems” (Anderson, et al., 1999). It is

extremely efficient in dealing with matrix operations. The subroutine `zsysv` that we adopted is used to solve complex linear equations:

“ZSYSV computes the solution to a complex system of linear equations $A * X = B$, where A is an N-by-N symmetric matrix and X and B are N-by-NRHS matrices. The diagonal pivoting method is used to factor A as $A = U * D * U^{**T}$, if UPLO = 'U', or $A = L * D * L^{**T}$, if UPLO = 'L', where U (or L) is a product of permutation and unit upper (lower) triangular matrices, and D is symmetric and block diagonal with 1-by-1 and 2-by-2 diagonal blocks. The factored form of A is then used to solve the system of equations $A * X = B$.” (Anderson, et al., 1999)

By using the `zsysv` LAPACK subroutine, the time to complete the same computation was reduced to 18 minutes.

3.4.2 MPI Parallelization

To gain as much performance as possible for the code, not only do we use the LAPACK subroutine instead of the numerical recipe subroutine, we also make use of MPI to run our code on clusters.

MPI, short for message passing interface, is actually a library specification for message-passing between processors. It was developed for high performance on parallel machines or workstation clusters. (Gropp, Lusk, & Skjellum, 1994)

In our model, many loops could be paralleled on, for example, the configuration loop, the angle loop, etc. We decided to parallel on the frequency loop, because we believe this way the model will run more efficiently without too much inter-processor message passing.

For a cloud of 3000 bubbles, it takes 48 minutes to compute one iteration on a single processor. After parallelization, it only takes 7 minutes to complete the same calculation on a node of 8 processors. The advantage of parallelization would be more obvious when we have even more bubbles, say 10,000, in a future simulation.

Chapter 4 Computation Scenarios

In this chapter, we apply the numerical model that we have developed to compute the cross section for a large number of bubbles, the corresponding resonant frequency shift, and phase distribution.

4.1 Scattering cross section for large number of bubbles

In scattering problems, the cross section is an important parameter which measures how much energy is scattered by the object. It is defined as:

$$\sigma = \int I \cdot r^2 d\Omega. \quad (42)$$

I is the intensity at radius r , Ω is the solid angle around the scatterer. According to the definition, the larger σ , the more energy the object scatters away, and the more effective as a scatterer the object is.

Here we calculate the cross section of the geometry outlined in Fig. 2, a spherical assemblage of N randomly distributed bubbles. The hard sphere assumption is applied in the problem, meaning that the minimum distance between any two bubbles should be larger than two times of the bubble radius.

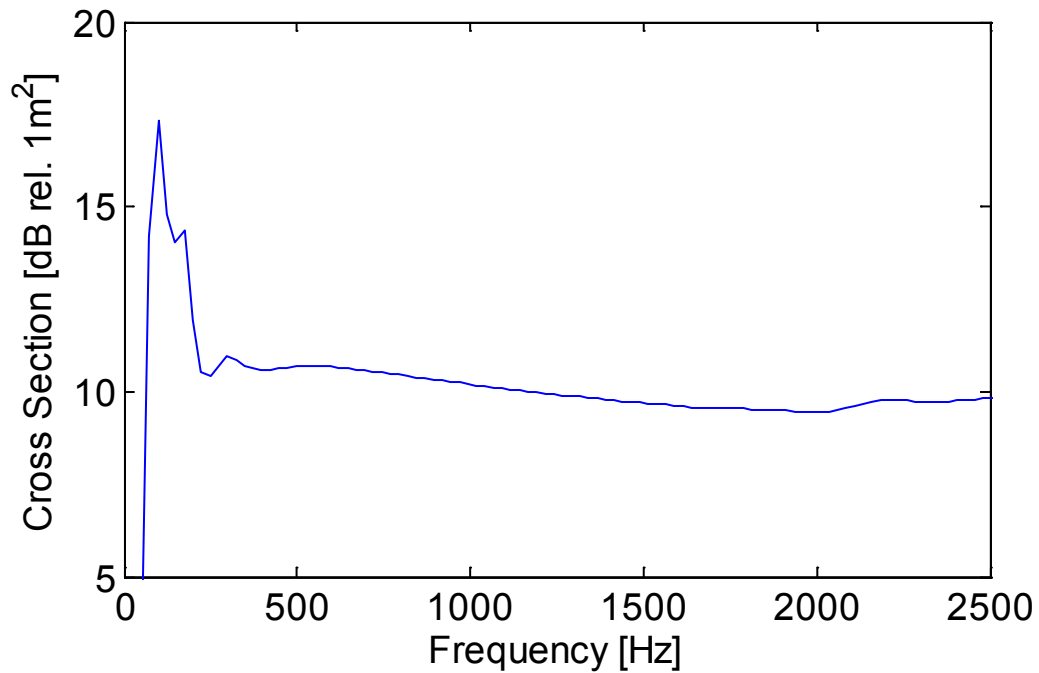


Fig. 3 Total scattering cross section of an assemblage consisting of 3000 bubbles. The void fraction β is 1%. The radius of the bubble is 0.0096 m, corresponding to a resonant frequency of 478 Hz. The radius of the assemblage is 0.34 m. The receivers are placed 4 m away from the assemblage.

Fig. 3 shows the total scattering cross section as a function of frequency ranging from 0 to 2500 Hz. Generally, the assemblage scatters more energy at lower frequencies, around 100 Hz, than higher frequencies. Moreover, the peak frequency of the total cross section is found near 100 Hz, which is much lower than 478 Hz the natural frequency of the bubble. This also supports the theory that the peak of ocean ambient noise spectrum around 500 Hz might be well connected to the multiple scattering effects from the surface bubble layer.

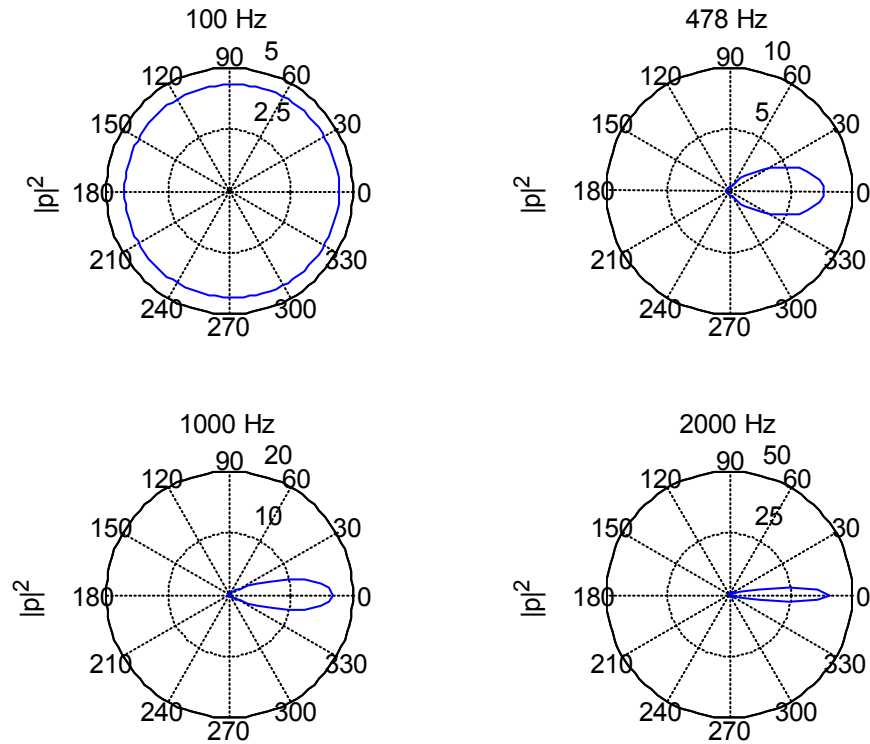


Fig. 4 Directivity of $|p|^2$ at 100 Hz (resonant frequency of the assemblage), 478 Hz (resonant frequency of a single bubble), 1000 Hz, and 2000 Hz.

Fig. 4 shows the scattering directivity of the spherical assemblage. 0 degree is the forward direction, and 180 degree is the backscattering direction. At low frequencies around 100 Hz, the directivity is quite uniform around all angles. However, as frequency increases, more energy is shifted from the backscattering direction to the forward direction. Meanwhile, since the total energy is constant, the amplitude in the forward direction also increases.

4.2 Resonant frequency shift

The resonant peak frequency of the total scattering cross section is an important parameter characterizing the multiple scattering effects of a bubble assemblage. As we have seen in Fig. 3, the resonant peak frequency for an assemblage of 3000 bubbles with void fraction of 1‰ is 98 Hz. The difference between the resonant frequency of an assemblage and the natural frequency of an individual bubble is believed to arise from the interaction between bubbles, i.e. the collective oscillations. To illustrate this point, consider a spring mass system. For a single spring, the natural frequency is $\sqrt{\frac{k}{m}}/2\pi$; for N springs in parallel, the natural frequency of the system is $\sqrt{\frac{k}{mN}}/2\pi$. The interaction among bubbles is more difficult to express quantitatively. So in this section, we will numerically simulate how the resonant frequency of an assemblage of bubbles varies with the number of bubbles N and the void fraction β .

The lowest collective mode of a bubble assemblage is considered to be the most important one. For an assemblage of N bubbles, the lowest mode of collective mode oscillation can be estimated with dimensional analysis (Commande & Prosperetti, 1989). First note that the approximate sound speed of the assemblage is given by the famous Wood's equation (Wood, 1964):

$$c_e^2 = \frac{P_0}{\rho_w \beta}. \quad (43)$$

Here β is the void fraction of the assemblage, $\beta = \frac{4}{3}\pi N a^3$, and L denotes the size of the assemblage. The lowest mode of the assemblage ω_e then can be estimated using the approximate formula $\omega_e \sim c_e/L$. Combining the above equations and inserting the Minnaert's equation for the natural frequency gives

$$\frac{\omega_e}{\omega_0} \sim \frac{1}{\beta^{1/6} N^{1/3}}. \quad (44)$$

According to the equation, the lowest collective mode of the assemblage decreases as the number of bubbles increases and the void fraction increases.

But in practical situations, the lowest mode of collective oscillation is not always the resonant peak of the cross section, especially in situations in which the density of the assemblage is high enough for multiple scattering effects to be taken into account, but not high enough for the collective modes to be the most prominent. In Hahn's paper, it is pointed out that at relatively high density of bubbles assemblages, the resonant frequency of total cross section might well be regarded as the lowest mode of collective

oscillation of the bubbles (Hahn, 2007).

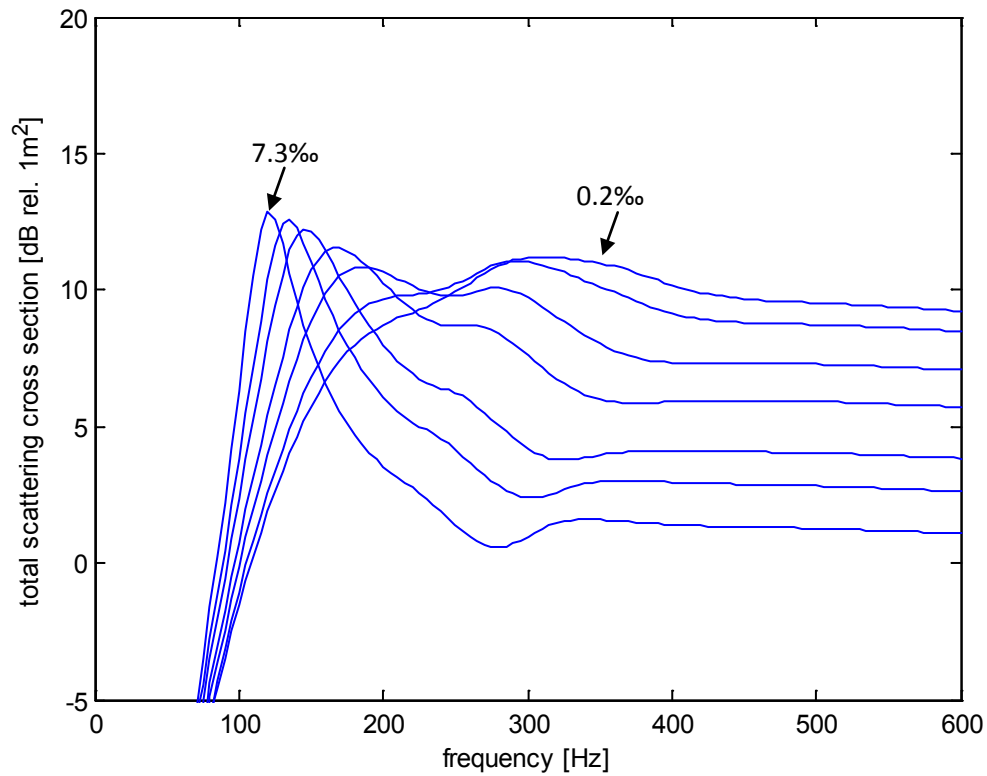


Fig. 5 Total scattering cross section for an assemblage of 500 bubbles.

From left to right, the void fraction goes from 7.3‰ to 0.2‰.

Fig. 5 shows the total scattering cross section for an assemblage of 500 bubbles. From left to right, the void fraction decreases from 7.3‰ to 0.2‰. From the figure, one sees that as the assemblage become dilute, the lower frequency resonance is inhibited and a second peak starts to emerge and grows rapidly. A steep jump in resonant frequency in Fig. 4 reflects such a transition of peak resonance.

Fig. 6 shows the relationship between resonant frequency and void fraction for different numbers of scatterers. This figure shows that as the void fraction increases, i.e. the cloud becomes more dense, the resonant frequency decreases.

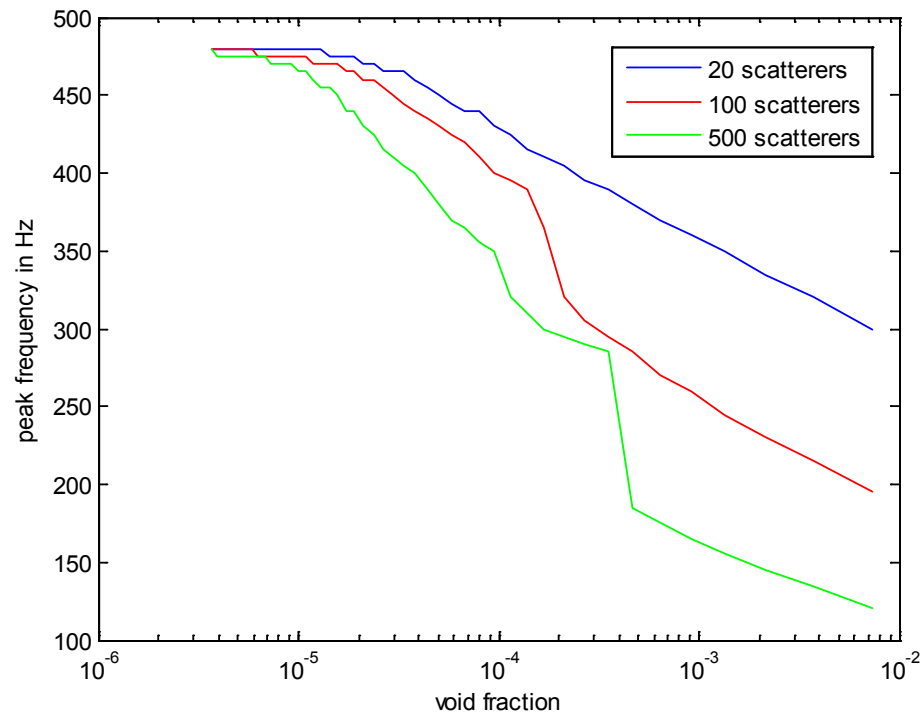


Fig. 6 Resonant frequency of assemblages of different void fraction values. Different numbers of scatterers are considered. The natural frequency of an individual bubble is 478 Hz.

When the assemblage is dilute enough (void fraction is less than 10^{-5}), the resonant frequency is approximately the natural frequency of a single bubble. This suggests that when void fraction is of order 10^{-5} , multiple scattering effects can be ignored. Otherwise, it needs to be taken into consideration. Also, it is shown in the figure that for assemblages of larger number of bubbles, void fraction is less as the resonant frequency

begins to reach the bubble's natural frequency. This can be interpreted that for even the same void fraction value, if the assemblage contains more bubbles or scatterers, more influence from the multiple scattering effects can be expected.

Also, though we are not sure if the resonant peaks at high void fractions (10^{-3} to 10^{-2}) in the figure are the lowest modes of the collective oscillation, an estimate from the data we have leads to the relationship that:

$$\omega_e \sim \frac{1}{\beta^{0.13} N^{0.29}}. \quad (45)$$

This is a very good approximation to the result from dimensional analysis.

To summarize this section, the resonant frequency of an assemblage of bubbles is sensitive to the interaction between bubbles. The more interaction between bubbles, i.e. the more numbers of scatterers or the closer the scatterers become, the lower the resonant frequency. When the interaction among bubbles is strong enough, the resonant frequency appears at the lowest collective mode of the assemblage. On the other hand, if the assemblage is dilute enough, the resonant frequency would appear at the natural frequency of an individual bubble.

4.3 Phase distribution

One of the most important features of this numerical tool is that it follows some first principles of physics, so that we can calculate the sound field by rigorously solving a system of equations instead of approximating effective parameters for the assemblage. This way we are able to see what is going on inside the assemblage. For example, we

may investigate the phase states of each bubble as they oscillate, which cannot be achieved otherwise.

The phase information of each bubble can be easily extracted from the derivation we presented in section 3.3. As we solve the matrix equation (38) to get the scattering field of the assemblage, one byproduct of the solution is the sum of scattering waves from all the other bubbles ($i = 1, 2 \dots N; i \neq j$) on bubble j , denoted as $p^i(\mathbf{r}_j)$. $p^i(\mathbf{r}_j)$ is complex valued and thus contains both amplitude and phase information. Now we can extract the phase information of the oscillating bubble j from $p^i(\mathbf{r}_j)$.

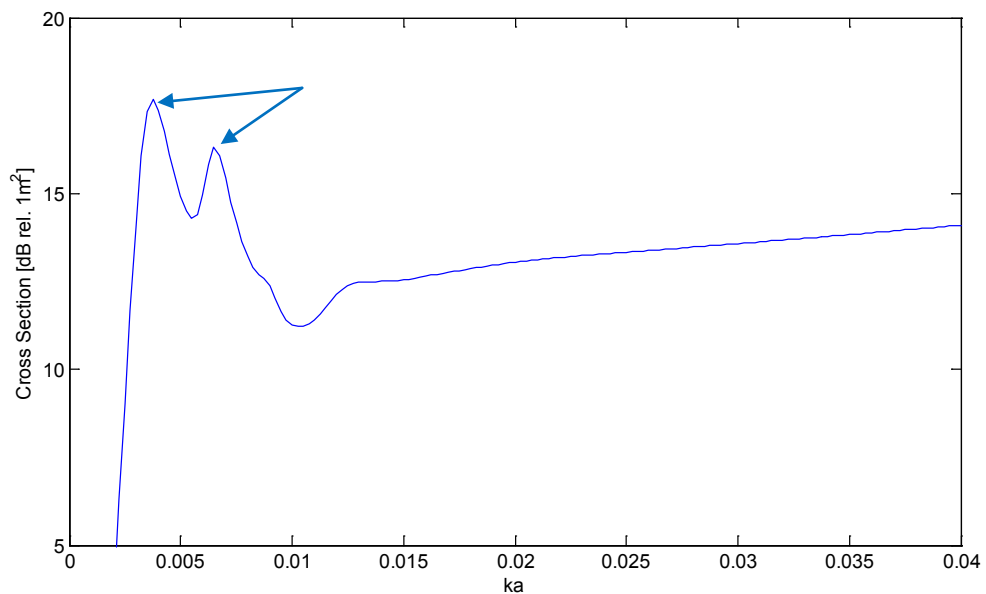


Fig. 7 Total scattering cross section as a function of ka .

Fig. 7 shows a typical plot for total scattering cross section as a function of ka , as discussed in section 4.1. Two resonant peaks can be easily recognized in the plot. From our numerical simulation, we were able to monitor the oscillation phase of each bubble

at these two resonant peaks. Fig. 8 shows the phase distributions for the two peaks. In the first peak, we can see that almost all bubbles synchronize their phases to the same value, about 1.5 rad, while the phase of the incoming wave at $x = 0$ is set to 0 rad. This result supports the claim that the first peak might be the lowest collective mode of the assemblage. In the second peak, phase synchronization is not present. But we do see that the phases of most bubbles are distributed nearby two states, 0 and 3 rad.

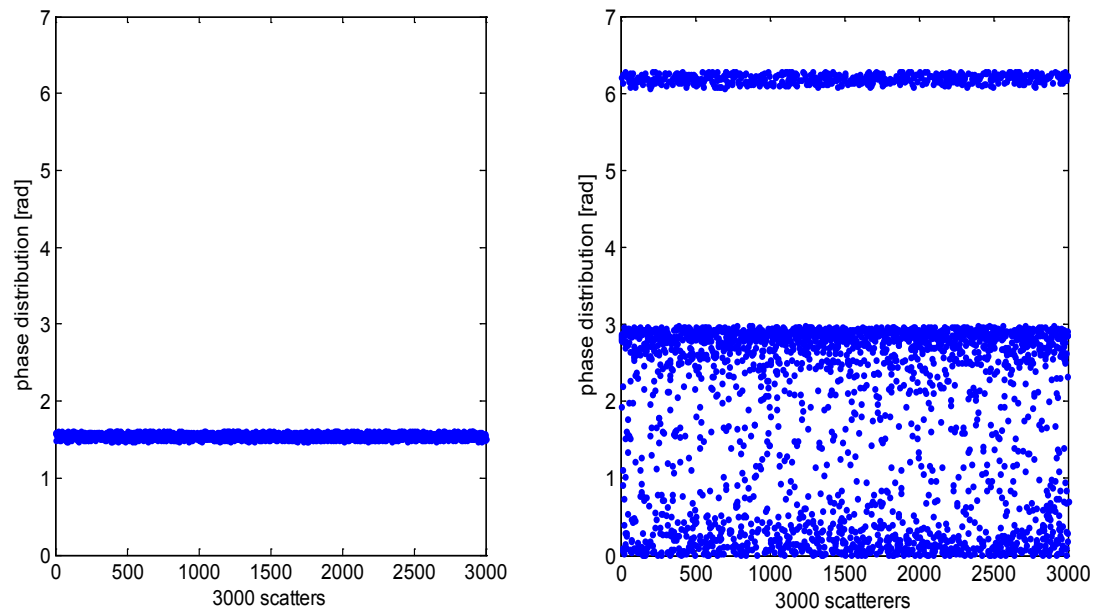


Fig. 8 Phase distribution of 3000 bubbles at two resonant peaks shown in Fig. 7

The preceding discussion considers only the scattered field. We may also take a look at the total field around the assemblage.

In the total field problem, the same geometry with previous problems is applied: there are 3,000 bubbles randomly distributed inside the assemblage; the void fraction is 1%. The only difference here is that we use a different source in this problem. Since in

the far field, the incoming plane wave hardly attenuates while the scattered wave attenuates with distance, we may use a point source at the center of the assemblage instead of a plane wave source. The point source would emit a monochromatic wave of angular frequency ω from inside the assemblage.

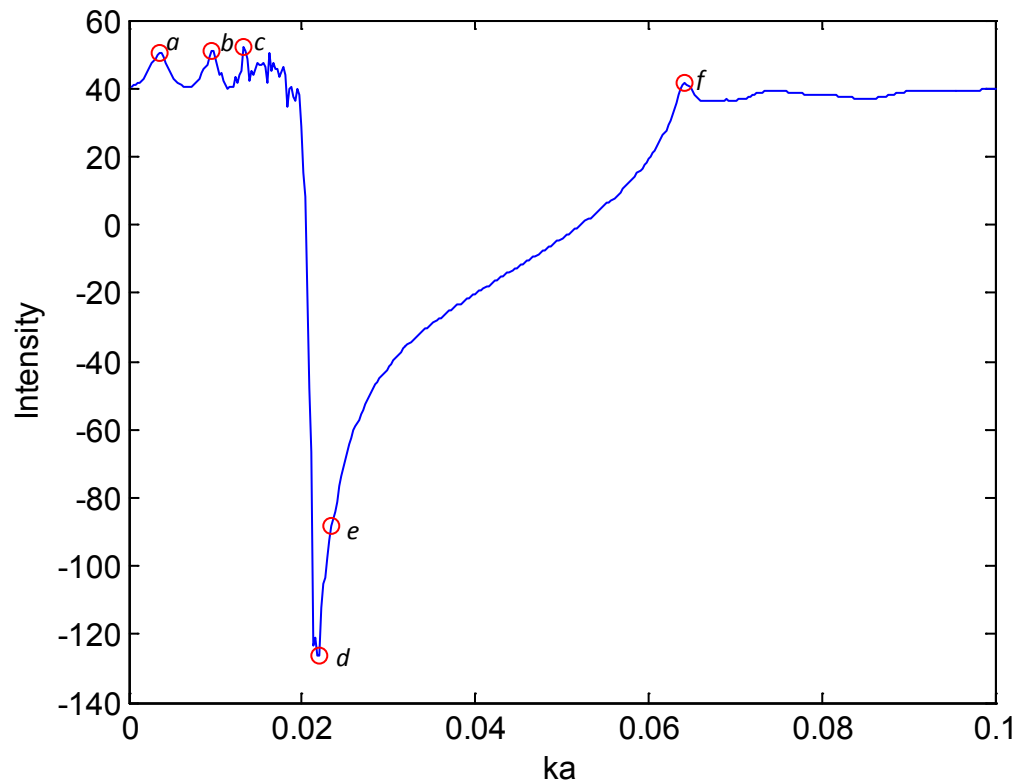


Fig. 9 Total field intensity level (compensated by distance, which is $r^2 \cdot I$), at different frequencies.

Fig. 9 is a plot of the total field intensity level far away from the assemblage. Special points of interest a to f are marked out in the plot. The peaks might correspond to different collective modes of the assemblage. Also notice that there is sharp decrease in

intensity level around $ka=0.0235$. The intensity level drops very quickly from 40 dB to -120 dB, which is almost undetectable.

Hoskinson & Ye (Hoskinson & Ye, 1999) reported similar results in their paper for a 2D case. They regard the sharp decrease as wave localization, which is analogous to the famous “electron localization” effect first found by Anderson in 1958 (Anderson P. W., 1958). When wave localization takes place, energy is basically trapped in one region until dissipated. Localization is thought to be associated with the process of multiple scattering.

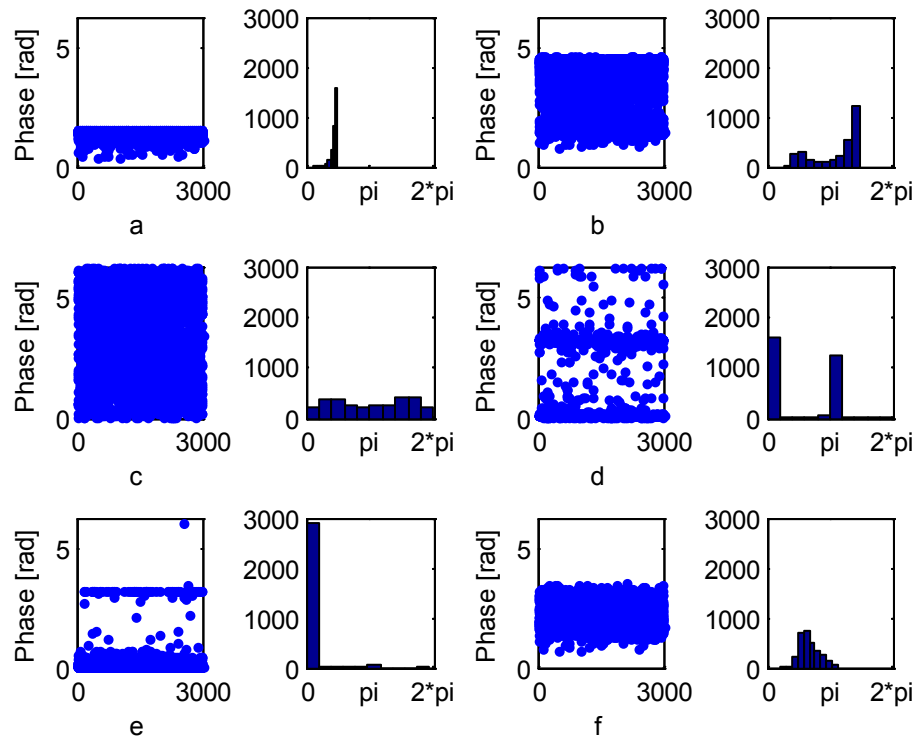


Fig. 10 Phase state distribution of the bubbles at frequencies marked out in Fig. 9.

Fig. 10 gives out the phase distributions at the frequencies marked out in Fig. 4, from a to f. Case a basically corresponds to the first resonant peak in the previous plot; almost all bubbles synchronize their phase to $\pi/2$. In case b, half of the bubbles' phases are near $3\pi/2$, while the rest is evenly distributed from $\pi/2$ to $3\pi/2$. In case c, though we do see a resonant peak in the plot, the phase states of the bubbles distribute randomly from 0 to 2π .

The most interesting phase distribution is case d, where wave localization is assumed to take place. As we can see, all the bubbles are split into 2 parts, half of them oscillate at phase 0 and the other half oscillate at phase π . In this situation, the two halves of bubbles are acting like 2 large bubbles oscillating π out of phase with each other, which can be regarded as a dipole.

An intuitive interpretation on the phase distributions can be given regarding resonant peaks and wave localization phenomena. In case (a), the phase states of almost all the bubbles tend to be synchronized at $\pi/2$, which means that almost all the bubbles in the assemblage contract and expand at the same phase. So as a whole, the assemblage emits energy very efficiently. However, in case (d), half of the bubbles oscillate π out of phase with the rest half. In this case, as half of bubbles expand, the other half contract. Basically, the water mass stays inside the assemblage and thus little energy is transmitted out. Of course, this is just a tentative explanation of the numerical result. The real story happening inside the assemblage might be much more complicated than we think.

Chapter 5 Summary

In this study, we have developed an efficient numerical model for general purpose calculations of multiple scattering effects in large number of scatterers. We applied our code in 3 scenarios:

1. Computing total coherent cross section for large number of bubbles. In this computation, we investigated the relationship between total coherent cross section and frequency. Several resonant peaks were recognized in the plot, which might be the collective modes of the bubble assemblage. The directivity of the scattering field is also studied. According to the data we obtained from the simulation, it was found that as the frequency increases, more energy is focused in the forward transmission direction.

2. Investigating the variation of resonant frequency shift. We computed the total coherent cross sections with different values of void fraction β and different numbers of scatterers N . It was found that as void fraction β increases, i.e. the assemblage becomes denser, the resonant peak frequency shifts down. A plot was given to quantitatively describe relationship between resonant frequency, void fraction, and the number of scatterers. It was also suggested from the plot that when the void fraction is below approximately 10^{-5} , multiple scattering effects do not play an important role.

3. Investigating the phase states of the oscillating bubbles in multiple scattering. With the help of our code, we can easily determine the phase states of each bubble in the assemblage. It is found that at some resonant peaks, all the bubbles seem to

synchronize to the same phase, which might suggest the lowest mode of collective oscillation. The phase states corresponding to the wave localization phenomenon was also investigated, and the results indicate that in this situation, half of the bubbles oscillate at phase 0 while the other half oscillate at phase π . An intuitive interpretation of this behavior was given.

Bibliography

- Anderson, E., Bai, Z., Bischof, C., Blackford, S., Demmel, J., Dongarra, J., et al. (1999). *LAPACK user's guide*. Philadelphia, PA: Society for Industrial and Applied Mathematics.
- Anderson, P. W. (1958). Absence of diffusion in certain random lattices. *Physical Review*, 1492-1505.
- Chen, Y.-Y., & Ye, Z. (2001). Theoretical analysis of acoustic stop bands in two-dimensional periodic scattering arrays. *Physical Review E* .
- Clay, C., & Medwin, H. (1977). *Acoustical oceanography: principles and applications*. New York: Wiley.
- Commande, K. W., & Prosperetti, A. (1989). Linear pressure waves in bubbly liquids: comparison between theory and experiments. *J. Acoust. Soc. Am.* , 732-746.
- Feuillade, C. (1995). Scattering from collective modes of air bubbles in water and the physical mechanism of superresonances. *J. Acoust. Soc. Am* , 1178-1190.
- Foldy, L. L. (1945). The multiple scattering of waves. *Physical Review* , 107-119.
- Gropp, W., Lusk, E., & Skjellum, A. (1994). *Using MPI*. London, England: The MIT Press.
- Hahn, T. (2007). Low frequency sound scattering from spherical assemblages of bubbles using effective medium theory. *J. Acoust. Soc. Am.* , 3252-3267.
- Henry, F. S. (1999). Corrections to Foldy's effective medium theory for propagation in bubble clouds and other collections of very small scatterers. *J. Acoust. Soc. Am.* , 2149-2154.
- Hoskinson, E., & Ye, Z. (1999). Phase transition in acoustic propagation in 2D random liquid media. *Physical Review Letters* , 2734-2737.
- Hughes, M., Klibanov, A. L., Marsh, J. N., Miller, J. G., & Brandenburger, G. H. (2000). Broadband time domain reflectometry measurement of attenuation and phase velocity. *J. Acoust. Soc. Am.* , 813-820.
- Leighton, T. (1994). *The Acoustic bubble*. London: Academic Press.
- Nicholas, R. R. (1994). Sound emissions by a laboratory bubble cloud. *J. Acoust. Soc. Am* , 3171-3182.
- Minnaert, M. (1933). On musical air-bubbles and sounds of running water. *Phil Mag* , 235-248.

Press, W. H., Teukolsky, S. A., Vetterling, W. T., & Flannery, B. P. (1992). *Numerical recipes in C*. New York: Cambridge University Press.

Prosperetti, A. (1988). Bubble Dynamics in oceanic ambient noise. In B. R. Kerman, *Sea surface sound* (pp. 151-171). Kluwer Academic Publishers.

Prosperetti, A. (1988). Bubble-related ambient noise in the ocean. *J. Acoust. Soc. Am.* , 1042-1054.

Twersky, V. (1962). On scattering of waves by random distributions. *Journal of Mathematical Physics* , 700-715.

Wenz, G. M. (1962). Acoustic ambient noise in the ocean: spectra and sources. *J. Acoust. Soc. Am.* , 1936-1956.

Wood, A. B. (1964). *A textbook of sound, 3rd edition*. London: Bell & Sons.

Ye, Z., & Ding, L. (1995). Acoustic dispersion and attenuation relations in bubbly mixture. *J. Acoust. Soc. Am.* , 1629-1636.

Ye, Z., Hsu, H., & Hoskinson, E. (2000). Phase order and energy localization in acoustics propagation in random bubbly liquids. *Physics letters A* , 452-458.

Yoon, S. W., Crum, L. A., Prosperetti, A., & Lu, N. Q. (1991). An investigation of the collective oscillations of a bubble cloud. *J. Acous. Soc. Am.* , 700-706.

Zhang, D., Gong, X. F., Liu, J. H., Shao, L. Z., Li, X. R., & Zhang, Q. L. (2000). The experimental investigation of ultrasonic properties for a sonicated contrast agent and its application in biomedicine. *Ultrasound Med. Biology* , 347-351.